Pure & Appl. Chem., Vol. 58, No. 7, pp. 999–1014, 1986.
Printed in Great Britain.

INTERNATIONAL UNION OF PURE
AND APPLIED CHEMISTRY

MACROMOLECULAR DIVISION

COMMISSION ON POLYMER CHARACTERIZATON
AND PROPERTIES

WORKING PARTY ON STRUCTURE AND PROPERTIES
OF COMMERCIAL POLYMERS*

APPLICATION OF FRACTURE MECHANICS TO THE PREDICTION OF THE DUCTILE–BRITTLE TRANSITION

Prepared for publication by

C. B. BUCKNALL

Cranfield Institute of Technology
Cranfield, Bedford, UK

*Membership of the Working Party during the preparation of this report (1983–85) was as follows:

Chairman: H. H. Meyer (FRG); *Secretary*: D. R. Moore (UK); *Members*: G. Ajroldi (Italy); R. C. Armstrong (USA); C. B. Bucknall (UK); J. M. Cann (UK); D. Constantin (France); H. Coster (Netherlands); Van Dijk (Netherlands); M. Fleissner (FRG); H.-G. Fritz (FRG); P. H. Geil (USA); A. Ghijsels (Netherlands); G. Goldbach (FRG); D. J. Groves (UK); H. Janeschitz-Kriegl (Austria); P. B. Keating (Belgium); H. M. Laun (FRG); A. S. Lodge (USA); C. Macosko (USA); J. Meissner (Switzerland); W. Michel (France); A. Plochocki (USA); W. Retting (FRG); U. P. Richter (FRG); G. Schorsch (France); G. Schoukens (Belgium); J. C. Seferis (USA); J. M. Starita (USA); G. Vassilatos (USA); J. L. White (USA); H. H. Winter (USA); J. Young (Netherlands); H. G. Zachmann (FRG).

Application of fracture mechanics to the prediction of the ductile–brittle transition

Abstract - Eleven different laboratories have collaborated in a research programme on factors affecting the fracture resistance of injection moulded plaques, as measured in dart impact tests. Factors investigated were the presence of weld lines and ejector pin marks, the test temperature and the yield stress σ_y and fracture toughness K_{IC} of the polymer over a range of temperatures. Materials studied were high density polyethylene (HDPE), nylon 66 (PA 66), and two grades of polypropylene (PP), a homopolymer and a copolymer. A fracture mechanics analysis showed that welds formed in PA66 by head-on impingement of melt fronts behaved like surface cracks of length 250 μm. Polarised light microscopy revealed the presence in the PA66 mouldings of a distinctive layer of large spherulites running normal to the surface to a depth of 500 μm. This weld-line defect structure was associated with low-energy fractures in the dart impact test on PA66 plaques. Correlations between weld-line defects and low impact energy were also observed in HDPE and PP. Large defect sizes, low K_{IC}, and high σ_y all contributed to brittle fracture.

INTRODUCTION

Fracture mechanics has made considerable progress in recent years and has led, among other developments, to an improved understanding of the behaviour of plastics in the notched Charpy and Izod tests. However, the relevance of these studies to the performance of components in service is far from obvious, since components usually do not contain sharp cracks, and every effort is made in the design to avoid features that could nucleate cracks. For this reason, manufacturers have tended to place greater reliance on dart impact tests, in which a hemispherical head strikes a clamped or simply supported disc. Dart impact tests are seen as simulating more closely the conditions that the material will experience in service.

This paper is the third in a series concerned with the impact behaviour of thermoplastic mouldings, as observed in the dart impact test. The two previous papers from the IUPAC Working Party on "Structure and Properties of Commercial Polymers" describe experiments on polypropylene homopolymer and copolymer (1,2). They show that weld lines and ejector pin marks drastically reduce the dart impact energy in both materials. On the other hand, Charpy tests on specimens notched along the plane of the weld show no evidence of weakness in comparison with other areas of the moulding. The aim of the present study is to develop a better understanding of the nature of the weld defect and to determine whether this information about the weld can be used in conjunction with fracture mechanics data to predict the performance of the moulding in impact.

Participants in the programme are identified in the text by the following abbreviations:

BASF	BASF AG, Ludwigshafen-am-Rhein, Germany
BP	BP Chemicals Ltd., Penarth and Grangemouth, U.K.
BW	Borg-Warner Chemicals, Amsterdam, Netherlands
CIT	Cranfield Institute of Technology, Bedford, U.K.
Hoechst	Hoechst AG, Frankfurt, Germany
ICI	ICI plc, Welwyn Garden City and Wilton, U.K.
Monsanto	Monsanto S.A., Louvain-la-Neuve, Belgium
MP	Montepolimeri, Bollate, Italy.
RP	Rhone Poulenc, Aubervilliers, France.
Solvay	Solvay & Cie, Brussels, Belgium
TNO	TNO, Delft, Netherlands.

MATERIALS AND MOULDING

The four polymers used in this study were: Moplen T30S polypropylene homopolymer, supplied by Montepolimeri; Propathene GWM101 copolymer, supplied by ICI; Rigidex 075-60 high density polyethylene, supplied by BP; and Technyl A216 nylon 66, supplied by Rhone-Poulenc. The two polypropylene grades were the same materials as used for the two earlier studies in the series (1,2). In all four cases, a single batch of material was reserved for the work and supplied to all participants.

The mould illustrated in Fig. 1, which played an important part in the two previous studies, was used by RP to prepare mouldings of HDPE and PA66, in which there is a central weld, produced either by head-on flow (Type I plaque) or parallel flow (Type II plaque). The thickness of both plaques was 3.7mm. Moulding conditions were as follows:

	HDPE	PA66
Barrel Temperatures (°C)	205,205,210,200,200,N*	275,275,270,270,275,N*
Plasticisation (s)	25	22
Screw Speed (rpm)	100	100
Mould Temperature (°C)	40	68
Injection Pressure (bar)	70	100
Hold Pressure (bar)	170	140
Injection Time (s)	6	7
Hold Time (s)	24	18
Cooling Time (s)	58	55

*N indicates position of nozzle. Moulding conditions for the two PP materials are given in reference (2).

Single edge gated (SEG) and double edge gated (DEG) discs with a diameter of 100 mm and a thickness of 3.1 mm were moulded by ICI. Each disc has a central scar on one face, caused by the ejector pin. In the DEG discs, the gates are situated diametrically opposite to each other but the weld line is slightly displaced from its expected position along a diameter midway between the gates.

MODULUS AND YIELD STRENGTH

Modulus and yield stress were measured in tensile tests over a range of strain rates at several different temperatures. Specimens tested by BASF were machined from 2 mm sheet compression moulded at 180°C (HDPE), 200°C (PP copolymer), 220°C (PP homopolymer), and 270°C (PA66). The PA66 was conditioned for 7 days at 70°C and 62% RH in accordance with ISO/DP1110 (1983); the other polymers were conditioned for several days at 23°C and 50% RH. An electro-optical extensometer was used to measure strains in high speed tensile tests. Specimens machined from RP injection moulded plaques at 0° and 90° to the flow direction were tested by MP in tensile impact to determine yield stress, and short-term moduli were calculated from rebound experiments on three-point bend specimens as described by Casiraghi and Savadori (3,4).

The results are presented in Figs. 2-13. As expected, modulus and yield stress increase with increasing strain rate and decreasing temperature, whilst elongations at yield and at rupture decrease in most cases. There is little evidence of anisotropy in the injection moulded plaques. The lowest yield strain recorded is 0.025, whilst the highest strain rate is $7s^{-1}$, at which rate yielding occurs in 3.5ms. This time is similar to the duration of many dart impact tests. It may therefore be concluded that the data given are applicable either directly, or with a small extrapolation, to the analysis of impact behaviour.

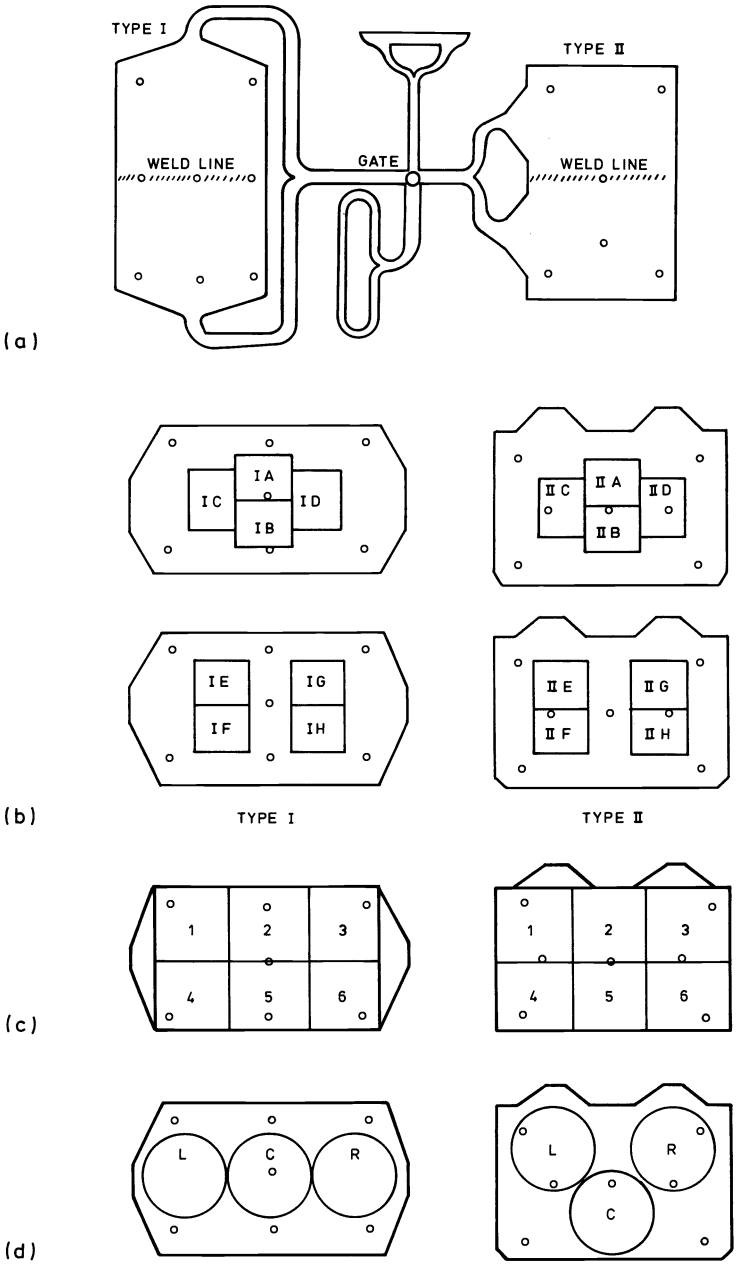

Fig. 1. (a) Rhone-Poulenc double-gated plaque mould, with cutting plan used by: (b) Monsanto, (c) ICI, and (d) MP.

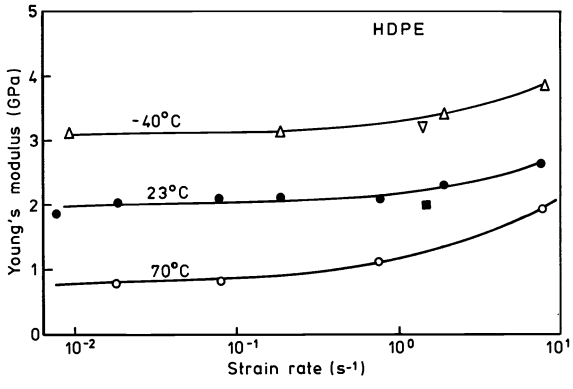

Fig. 2 Modulus of HDPE: (Δ, ●, ○) data of BASF; (▽, ■) data of MP.

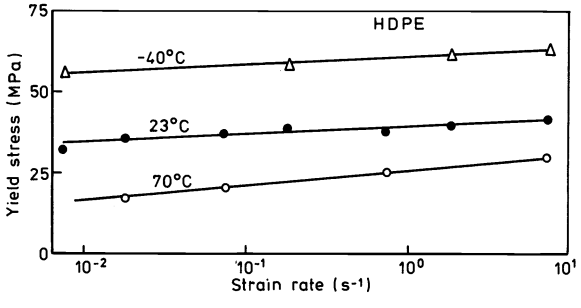

Fig. 3 Yield stress of HDPE. Data of BASF.

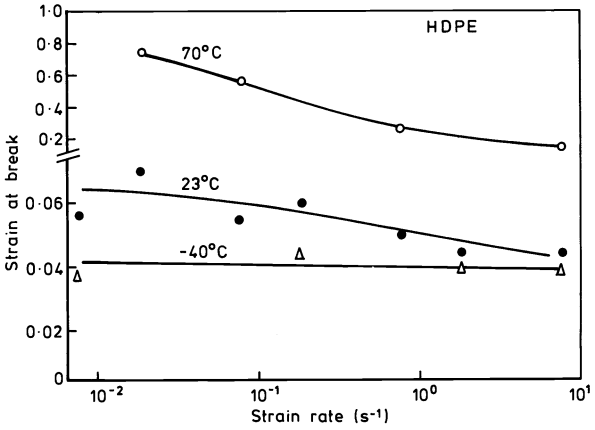

Fig. 4 Tensile elongation at break in HDPE specimens. Data of BASF.

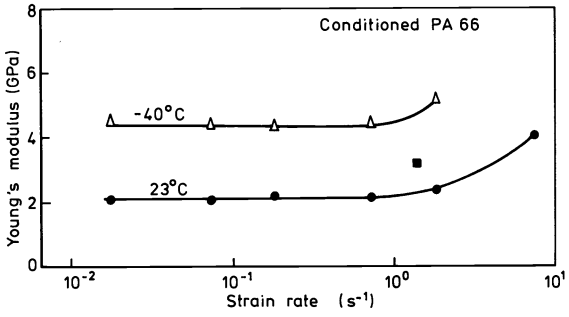

Fig. 5 Modulus of PA66: (Δ,●) data of BASF on conditioned specimens; (■) data of MP on dry specimens.

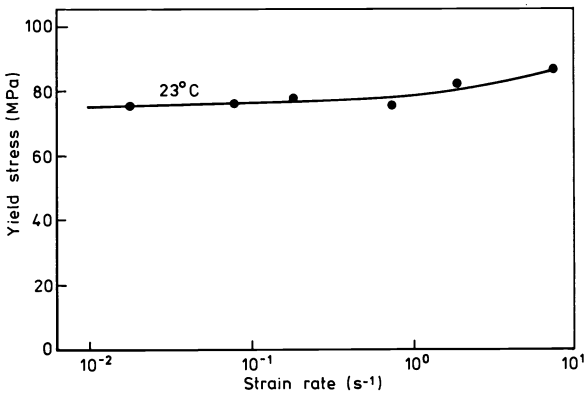

Fig. 6 Yield stress of conditioned PA66. Data of BASF.

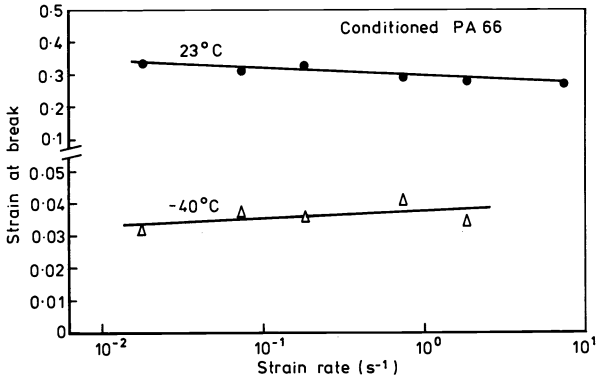

Fig. 7 Tensile elongation at break in PA66 specimens. Data of BASF.

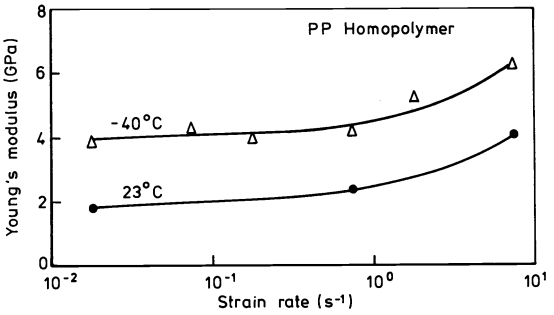

Fig. 8 Young's modulus of PP homopolymer. Data of BASF.

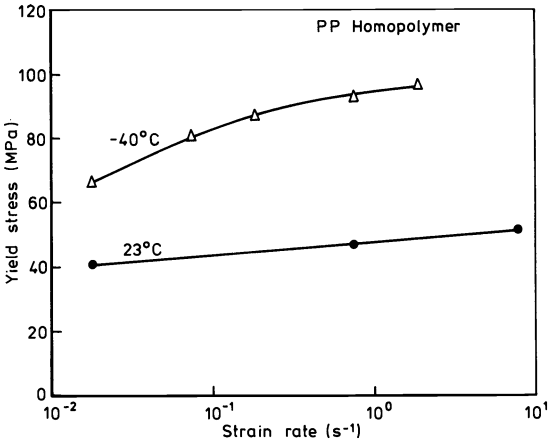

Fig. 9 Yield stress of PP homopolymer. Data of BASF.

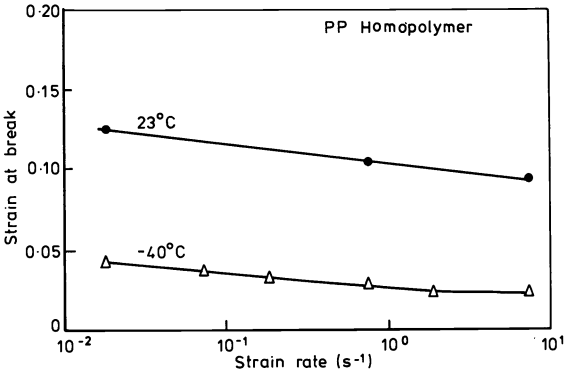

Fig. 10 Tensile elongation at break in PP homopolymer specimens. Data of BASF.

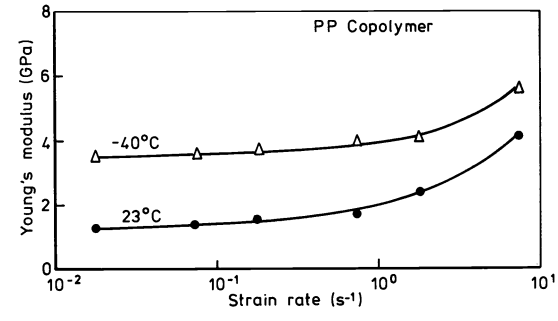

Fig. 11 Modulus of PP copolymer. Data of BASF.

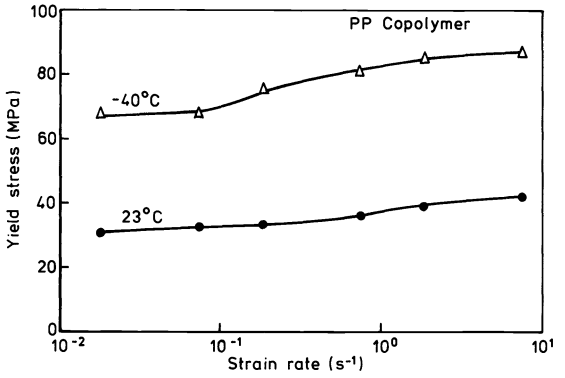

Fig. 12 Yield stress of PP copolymer. Data of BASF.

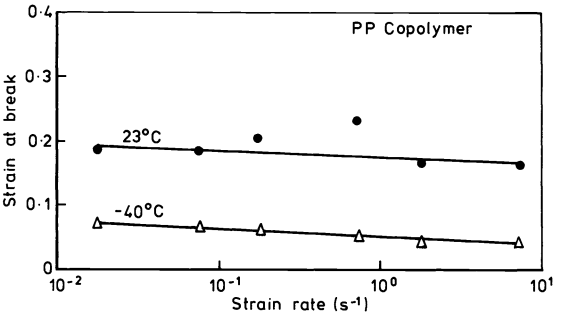

Fig. 13 Tensile elongation at break in PP copolymer. Data of BASF.

MEASUREMENT OF K_{IC} AND G_{IC}

Fracture mechanics results for the two polypropylenes are presented and discussed in the previous report on this programme (2). In the present study, data on HDPE and dry PA66 were obtained from Charpy impact tests on sharply-notched specimens machined from RP plaques (Fig. 1a). Hoechst and MP used instrumented pendulum equipment, whilst BP, Solvay and TNO relied upon measurements of total energy to break U_f. Values of K_{IC} were calculated from peak loads obtained from instrumented tests and G_{IC} was calculated from plots of U_f against $BW\emptyset$, where B and W are specimen thickness and width respectively and $\emptyset$ is the compliance factor according to Williams (5).

Non-linearity in plots of U_f against $BW\emptyset$, and in force-deflection curves from the instrumented tests, showed clear evidence of ductility in HDPE at temperatures above -50°C, especially when crack lengths were small. At 23°C, linear force-deflection curves were obtained only over a restricted range of a/W close to 0.3. A detailed study by MP on the applicability of LEFM to Charpy impact data led to the conclusion that measurements of U_f are an unsatisfactory basis for the determination of G_{IC} unless careful checks are carried out to ensure linearity in the force-deflection curve: one problem is insufficient stiffness in the impact testing machine, leading to errors that increase with the fracture resistance of the specimen. A major difficulty is that specimens taken from injection mouldings are limited in thickness. Chan and Williams studied the conditions necessary to obtain valid plane-strain values of G_{IC} and K_{IC} in SEN specimens of HDPE subjected to three-point bending (6), and concluded that for a span-to-width ratio S/W of 4, the minimum values of B and W are:-

$$B_{min} = 2.5 \left[\frac{K_{IC}}{\sigma_y} \right]^2 \quad \text{and} \quad W_{min} = 6.25 \left[\frac{K_{IC}}{\sigma_y} \right]^2 \qquad (1)$$

Taking K_{IC} of HDPE as 2.0 MPa.$m^{\frac{1}{2}}$ and using the yield stress values in Fig. 2 for the highest strain rate, these limits give estimated minimum values of B and W respectively as 6 and 16 mm at 23°C and 2.5 and 6 mm at -40°C. As the moulded plaques are 3.7 mm thick, the required specimen dimensions can be achieved only at low temperatures. Notches must be cut across the narrower face of the bar, allowing W to be larger than 6 mm: if B is large and W is 3.7 mm, the specimen will undergo extensive yielding on the net section next to the notch. Because of these problems of ductility, fracture mechanics data for HDPE are quoted only for instrumented impact tests at -70°C, in which linearity is observed in the force-deflection curve and specimen

dimensions meet the above requirements for plane-strain fracture. The results are given in Table I, which also includes data on nylon 66.

Dry PA66 does not exhibit the same degree of ductility in the notched Charpy test. Linear force-deflection curves are obtained at all test temperatures, including 23°C. The table shows that the nylon has a higher K_{IC} than HDPE at -70°C. The applicability of LEFM to dry nylon at 23°C can be attributed to a high yield stress rather than a low fracture toughness.

MICROSCOPY

Sections were microtomed from both Type I and Type II plaques of the two materials, especially in the weld line region, and examined between crossed polars. In HDPE, there is an oriented skin approximately 20 μm thick but a barely detectable difference in

TABLE 1. Tensile impact data for HDPE and dry PA66. Specimen axis along (A) or across (X) flow. Modulus E measured by rebound method at 0.1 m/s. All other tests at 1 m/s. Data of MP.

		Plaque Type	-70°C		23°C	
			A	X	A	X
HDPE	E (GPa)	I	3.30	3.30	2.03	2.05
		II	3.30	3.30	2.00	2.02
	σ_y (MPa)	I	72	72	43	43
	K_{IC}	I	2.7	2.6		
	(MPa.m$^{1/2}$)	II	2.7	2.7		
	G_{IC} (kJ/m^2)	I	2.2	2.1		
	from K_{IC}	II	2.2	2.1		
	G_{IC} (kJ/m^2)	I	2.6	2.6		
	from U_f	II	2.7	2.7		
PA66	E (GPa)	I	3.61	3.59	3.20	3.11
		II	3.47	3.59	3.16	3.13
	σ_y (MPa)	I	163	180	123	126
	K_{IC}	I	3.0	3.1	3.1	3.1
	(MPa.m$^{1/2}$)	II	3.2	3.2	3.1	3.1
	G_{IC} (kJ/m^2)	I	2.5	2.7	2.9	3.0
	from K_{IC}	II	3.0	2.9	3.0	3.1
	G_{IC} (kJ/m^2)	I	2.4	2.7	3.1	3.2
	from U_f	II	2.8	2.8	3.3	3.4

structure marking the position of the weld. In PA66 by contrast, the quenched skin varies in thickness between 30 and 45 μm, depending upon position in the moulding, and the weld line is clearly delineated. In Type I plaques in which the flow fronts meet head-on, the weld is marked by a region of large spherulites running to a depth of over 500 μm. The weld region in the PA66 specimens is approximately 25 μm thick and consists of 15 μm spherulites, whereas the average spherulite diameter in the surrounding polymer is about 6 μm. Near the moulded surface, the structure changes as shown in Fig. 14 : at a depth of 115 μm below the surface, the large spherulites give way to a very fine grained pattern which is succeeded at a depth of about 50 μm by a largely featureless zone in which the junction between the two melt fronts can clearly be seen. In Type II plaques, by contrast, the weld region is much less distinct. A band approximately 12 μm thick containing 8 μm spherulites can just be distinguished to a depth 500μm below the surface, and a V-notch with a depth of 20 μm can be seen at the surface in some areas where the melt fronts have not closed up to the mould wall.

From these microscopy studies and from the high fracture energies G_{IC} recorded at the weld, there are grounds for concluding that the weld behaves in a similar manner to a surface crack, rather than a through-thickness weakness. It follows that an equivalent crack length a_o can be assigned to the weld by measuring the energy to break U_o in unnotched Charpy tests on specimens from the weld region, and using the relationship between U and $BW\emptyset$ from the G_{IC} determination to calculate $\emptyset_o$ and hence a_o. This principle was applied to the present investigation. Unnotched bars of HDPE and PA66 were machined from the weld region and from other parts of the RP plaques. In tests over a range of low temperatures, BP and Hoechst showed that brittle fracture occurred at the weld in Type I plaques of PA66, but that PA66 specimens from other areas, and all of the HDPE specimens, were resistant to fracture. Individual values of a_o from single tests showed a high degree of scatter but mean values obtained in three sets of tests, each on ten specimens, were remarkably consistent: BP estimated a_o to be 230 μm from tests at -20°C; whilst Hoechst estimated 240 μm (at 23°C) and 300 m (at -70°C).

A 5 μm thick section of the weld region from a Type I plaque of the PP homopolymer is shown in Fig. 15. The section is taken from the centre of the moulding, opposite the ejector pin marks. Birefringence measurements made by Hoechst indicate that this side has the lower surface orientation in the flow direction, normal to the weld. The micrographs showed an oriented quenched skin, approximately 40 μm thick, and with no detectable spherulitic structure. Below this skin, spherulites increase in size towards the core of the moulding. The region of the weld is marked by an apparently non-spherulitic triangular feature with its apex in the surface and a base about 100 μm long at a depth of 120 μm below the surface.

Fig. 14 Polarised light micrograph taken by BP, showing the weld region in a section from a Type I PA66 plaque.

Fig. 15 Polarised light micrograph taken by Hoechst, showing the weld region in a section from a Type I PP homopolymer plaque.

Hoechst machined unnotched Charpy bars from these Type I plaques of PP homopolymer and tested them at -20°C using an instrumented pendulum. All fractures were essentially brittle. Load-deflection curves were linear for specimens containing a weld, but slightly non-linear for specimens cut from other parts of the plaque. Defect sizes a_o were calculated from peak loads, using a K_{IC} of 1.7 MPa.m$^{\frac{1}{2}}$ for PP (2). Good reproducibility was obtained giving a_o = 90 μm at the weld and a_o = 40 μm at other positions in the plaque: these figures are in good agreement with the dimensions of the weld zone and the thickness of the quenched surface, as observed in the optical microscope.

Scanning electron micrographs taken by MP of the fracture surfaces of PP tensile impact specimens confirm that the weld lines act as crack initiators in both homopolymer and copolymer. Both show planar initiation zones running parallel to the moulded surface. Where the surface has been machined away to a depth of 200 μm, or where there is no weld, cracks initiate at points that are often not on the specimen surface.

DART IMPACT TESTS ON HDPE AND PA66 PLAQUES

Monsanto measured impact energies of plate specimens cut from RP plaques according to the plan shown in Fig.1b. Specimens were clamped between rings with an inside diameter of 63.5 mm and tested at 22°C in an instrumented driven-dart machine, in which a 38 mm diameter hemispherical striker is driven from the ejector pin side through the specimen at a constant speed of 1.01 m/s. The results are presented in Fig. 16 and 17 in the form of histograms.

The two materials differ strongly in their behaviour. Most of the failures in HDPE are closely grouped together, with energies to fail between 225 and 350J. This population of essentially ductile failures includes all six of the specimens from the weld region of Type I plaques. However, the remaining three specimens from Type I plaques, in which the melt fronts meet head-on, show a distinct weakness at the weld.

The distribution of failure energies is much broader for PA66, with a minimum of 26J, maximum of 984J, and a mean of 322J. Again, the Type I plaque shows a marked weakness at the weld line, with failure energies ranging from 26 to 35J. Type II plaques show no such weakness: failure energies at the weld are distributed throughout the

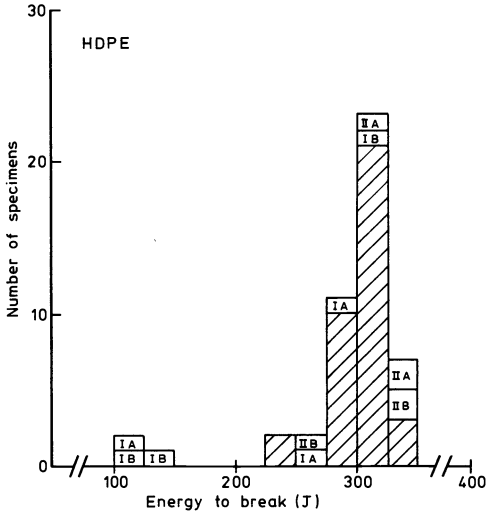

Fig. 16 Histogram of impact energies in driven dart tests on the HDPE specimens illustrated in Fig. 1(b). Specimens containing weld lines (IA, IB, IIA, IIB) are distinguished from those without a weld (I and II, C to H), which are represented by the shaded columns. Data of Monsanto.

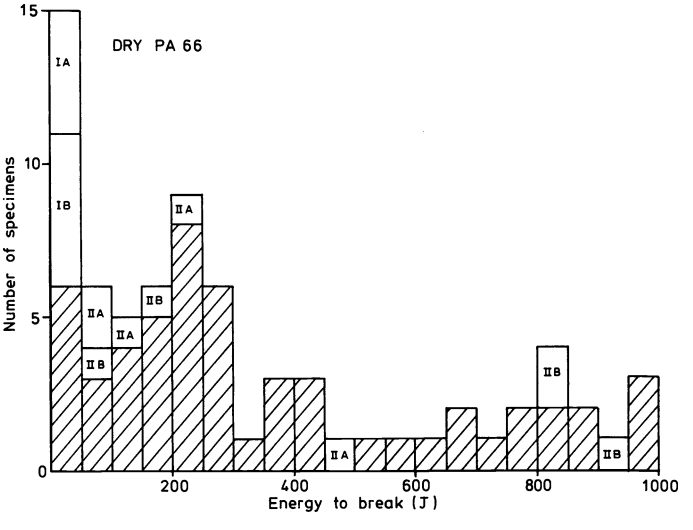

Fig. 17 Histogram of impact energies in driven dart tests on PA66. Symbols as in Fig. 16. Data of Monsanto.

population and the mean energy is 372J, which is higher than the mean for the population as a whole. If specimens from the weld region of Type I plaques are excluded from the calculation, the population mean is 360J.

In a second series of driven-dart tests by Monsanto, the clamping rings had an inside diameter of 57 mm and the striker speed was 2.64m/s, with a head diameter of 38 mm as before. Specimens were taken from the same positions in the RP plaques as in the first series. The pattern of results is broadly similar. In HDPE, the mean failure energy of 93 specimens was 249J, with a minimum, away from the weld region, of 194J, and a maximum of 306J; whereas at the weld in Type I plaques, impact energies were between 140 and 213J. In these experiments, the plaques were tested with the ejector pin marks both on the upper and lower side of the specimen and showed a 6% lower failure energy when struck from the ejector pin side. In PA66, the weld region of Type I plaques is again distinctly weaker than any other area and the remaining specimens show a wide range of failure energies.

In the ICI instrumented impact tests, specimens taken from RP plaques, as shown in Fig. 1c, were simply supported on a 50 mm diameter ring and struck with a 12.7 mm diameter head at an impact velocity of 5 m/s. For test temperatures below 0°C, specimens were immersed in a mixture of solid carbon dioxide and methanol until temperature equilibrium was achieved; and for 0°C and above (including 23°C), specimens were immersed in water at the test temperature. Failures were classified as: (D) ductile; (DB) mainly ductile but with some degree of brittleness; (BD) mainly brittle but with some signs of ductility; and (B) brittle. The results are summarised in Tables 2 and 3. In Type I plaques, the weld line causes a small reduction in the failure energy of HDPE and a very large reduction in the failure energy of PA66. In Type II plaques, on the other hand, the weld line has no significant effect on fracture energy. Reducing the test temperature results in an increase in the failure energy of the basically ductile HDPE, whereas it causes a reduction in the impact energy of the more brittle PA66. The reason for the difference is clear from Figs. 18 - 21. The yield stress of HDPE increases as the temperature is reduced, as illustrated in Fig. 3, causing an increase in the load maximum and total energy absorbed in the dart impact test. A similar increase in yield stress is observed in PA66 on lowering the temperature, but in this material the main effect is to increase the proportion of brittle fractures so that average impact energies drop.

The effects of temperature were also studied by ME, using a 60 mm diameter clamping ring and a 20 mm diameter hemispherical striker head at an impact velocity of 4.4 m/s. Disc specimens were machined from RP plaques according to the plan shown in Fig. 1d. The pattern of failures is broadly as observed by other participants and is illustrated in Figs. 18-21. In HDPE, failures are essentially tough and ductile, except for the central region of Type I plaques which contains the weld. At -70°C, the energy delivered by the striker (77J) is insufficient to puncture discs from Type II plaques, or from Type I plaques away from the weld. At -20°C, yielding occurs at a lower applied load and is followed by the formation of a short tear in the most highly strained area. At 23°C, the maximum load is lower again and there is a greater amount of yielding before the striker punctures the disc. Some of the specimens from the weld region of Type I plaques show the same ductile response as the remainder of the discs but approximately half of them show a sharp load drop at, or just beyond, the point of maximum load, as a crack propagates across the diameter; at -70°C, this rapid release of energy is sufficient to shatter the disc into many pieces.

In PA66, the MP tests show a wide range of behaviour over the temperature range 0-60°C. As in HDPE, the load maximum in ductile failures decreases with increasing temperature, reflecting the decrease in yield stress. At 0°, 23° and 40°C, all of the specimens from Type II plaques and from the central (weld) region of Type I

TABLE 2. Dart impact data for HDPE. Results of ICI on RP plaques.

Specimen Position (Fig. 1c)	T (°C)	Mean Failure Energy (J)	Failure Mechanism
	Plaque Type I		
1,3,4,6	-60	43.4	4D/8DB
2,5	-60	37.8	1D/5DB
1,3,4,6	-40	40.4	10D/2DB
2,5	-40	30.8	2D/2DB/1BD/1B
1,3,4,6	23	35.5	24D
2,5	23	28.9	8D/2DB/2BD
	Plaque Type II		
1,3,4,6	-60	39.7	7D/4DB/1BD
2,5	-60	44.9	5D/1DB
1,3,4,6	-40	39.7	12D
2,5	-40	40.7	6D
1,3,4,6	23	34.4	11D/1DB
2,5	23	33.9	6D

TABLE 3. Dart impact data for PA66. Results of ICI on RP plaques.

Specimen Position (Fig. 1c)	T (°C)	Mean Failure Energy (J)	Failure Mechanism
	Plaque Type I		
1,3,4,6	-40	14.7	12B
2,5	-40	3.0	6B
1,3,4,6	23	56.5	8D/4B
2,5	23	2.5	6B
	Plaque Type II		
1,3,4,6	-40	14.0	12B
2,5	-40	21.1	1D/5B
1,3,4,6	23	59.5	9D/3B
2,5	23	51.5	4D/2B

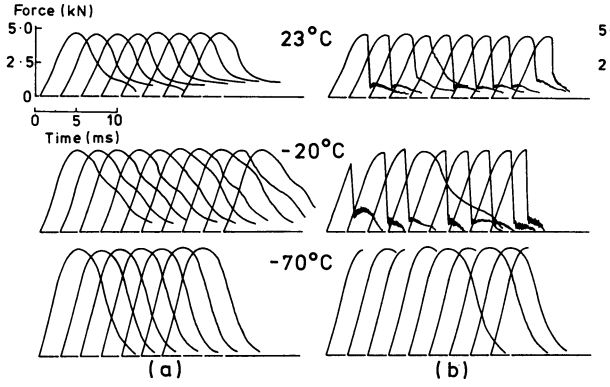

Fig. 18 Force-time curves from instrumented dart drop tests on discs cut from Type I HDPE plaques. (a) discs from left and right of plaque (see Fig. 1d); (b) discs from centre weld region. Data of MP.

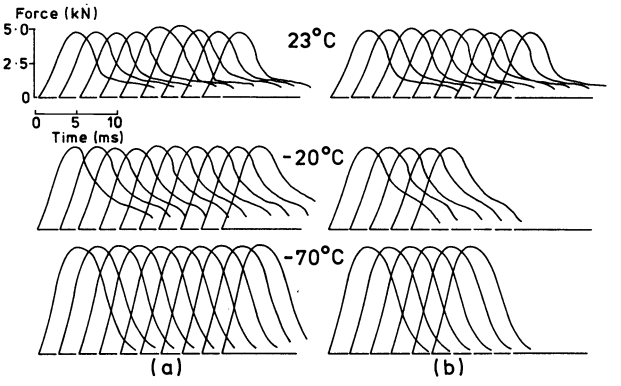

Fig. 19 Force-time curves from instrumented dart drop tests on discs cut from Type II HDPE plaques. (a) left and right of plaque; (b) centre of plaque. Data of MP.

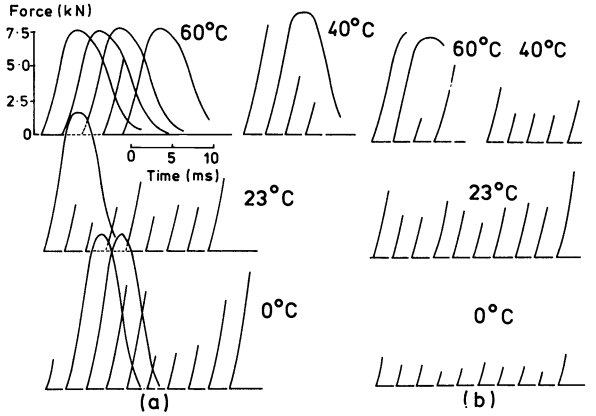

Fig. 20 Force-time curves from instrumented dart-drop tests on discs cut from Type I dry PA66 plaques. (a) left and right of plaque; (b) centre of plaque. Data of MP.

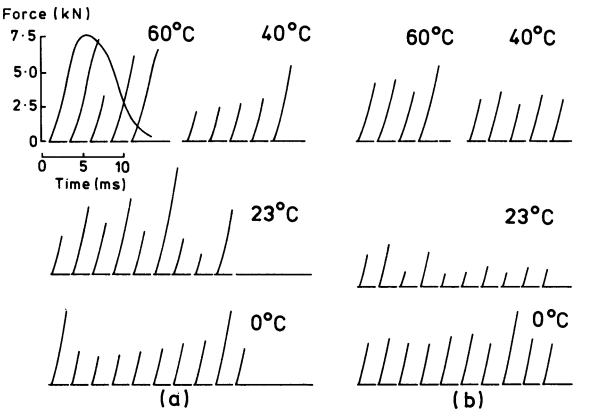

Fig. 21 Force-time curves from instrumented dart-drop tests on discs cut from Type II dry PA66 plaques. (a) Left and right of plaque. (b) Centre of plaque. Data of MP.

plaques fracture before reaching general yield. By contrast, specimens from the left and right hand sides of Type I plaques show a mixture of brittle and ductile behaviour. The majority of specimens from the central region of Type II plaques form circular cracks concentric with the point of impact rather than fracturing along the weld line. These cracks initiate at an ejector pin mark, which is on the side facing the striker and close to the clamping ring, showing that the weld is not a major cause of weakness in Type II plaques.

DART IMPACT TESTS ON POLYPROPYLENE DISCS

Single edge gated (SEG) and double edge gated (DEG) discs of polypropylene homopolymer and copolymer were tested under the conditions described in Section 5. The discs have an average thickness of 3.1 mm and a prominent central scar between 0.3 and 0.6 mm deep caused by the ejector pin.

Monsanto tested five specimens of each type at 22°C, with the ejector pin mark facing the 38 mm diameter striker, using a 63.5 mm diameter clamping ring and a striker speed of 1.01 m/s. The results showed a relatively small reduction in impact energy caused by the weld; from 115 to 94 J in the homopolymer, and from 138 to 107 J in the copolymer.

Results obtained by ICI over a range of temperatures are summarised in Tables 4 and 5. Surprisingly, the DEG discs have higher failure energies than the corresponding SEG discs. However, the average impact energies throughout both sets of specimens are substantially lower than usual for polypropylenes, possibly because of the exceptionally prominent pin scar.

Observations by Montepolimeri support the view that the ejector pin mark reduces fracture energy, although the impact is onto the mark itself. The reduction is particularly evident in the copolymer, as shown in Table 6; indeed, the impact energy of DEG specimens is actually lower in the copolymer than in the homopolymer at 50°C.

TABLE 4. Dart impact data for PP homopolymer. Results of ICI for ICI discs.

T (°C)	Number of Specimens	Mean Failure Energy (J)	Failure Mechanism
	Disc Type SEG		
23	10	3.0	10B
40	5	8.3	1B/3BD/1DB
60	5	13.7	2D/1DB/1BD
	Disc Type DEG		
23	10	3.7	10B
60	5	16.0	2D/3DB

TABLE 5. Dart impact data for PP copolymer. Results of ICI for ICI discs.

T (°C)	Number of Specimens	Mean Failure Energy (J)	Failure Mechanism
	Disc Type SEG		
0	5	2.3	5B
10	5	9.1	5BD
23	10	3.8	10BD
30	5	4.7	5BD
40	5	10.0	3D/1DB/1BD
60	5	10.7	4D/1DB
	Disc Type DEG		
23	10	5.2	5B/5DB
60	5	13.2	2D/1DB/1BD

TABLE 6. Dart impact energy (J) of SEG and DEG discs prepared by ICI. Data of MP.

	PP Homopolymer		PP Copolymer	
	SEG	DEG	SEG	DEG
0°C	0.43	0.40	8.6	2.2
23°C	6.4	3.5	24.6	4.4
50°C	24.6	15.8	> 77	10.5

ANALYSIS OF THE DART IMPACT TEST

In the most general case, the response of a disc to dart impact passes through four stages: an initial elastic deflection; first yield at the point of maximum stress; more general yielding under the striker head and in other areas of high stress; and, finally, tearing.

Elastic response

Solutions are available in standard tests for the elastic deformation of a disc under central point loading. However, these solutions lead to impossibly high (or infinite) stresses immediately under the load and it is, therefore, necessary to modify the analysis if a calculation of the maximum stress is required. The problem has been studied by Bucknall and Galloway (7). The area of contact between the striker and the disc is given by Hertzian contact theory (8) as:

$$b = \left[\frac{3}{4}\,\frac{P\,R\,(1-\nu^2)}{E}\right]^{\frac{1}{3}} \qquad (2)$$

where b = radius of contact surface, P = force exerted by striker, R = radius of striker head, ν = Poisson's ratio of polymer, and E = Young's modulus of polymer. Poisson's ratio, which has not been measured in the programme, is typically 0.4 for rigid polymers and this value will be used in calculations.

The distribution of pressure P_r at a radial distance r from the axis of striker is given by:

$$P_r = \frac{1.5P}{\pi b^3}\sqrt{b^2 - r^2} \quad \text{for } 0 \leqslant r \leqslant b \qquad (3)$$

The force exerted by the striker produces flexural stresses in the disc, which are highest in the surfaces of the disc. The radial stress σ_r in the surface of a clamped disc may be calculated from equation (2) using solutions for a disc subjected to loading of an annulus concentric with its axis (9), and integrating over the contact area. Immediately below the centre of the striker, at r = 0:

$$\sigma_r = \frac{3P(1+\nu)}{4\pi t^2}\left[2\log_e\left(\frac{a}{2b}\right) + \frac{5}{3} + \frac{2b^2}{5a^2}\right] \qquad (4)$$

where a is the internal radius of the clamp ring and t is the thickness of the disc. More generally, for r > b:

$$\sigma_r = \frac{3P}{4\pi t^2}\left[2(1+\nu)\log_e\left(\frac{a}{r}\right) - 2 + \frac{2b^2}{5}\left(\frac{1+\nu}{a^2} + \frac{1-\nu}{r^2}\right)\right] \qquad (5)$$

Taking ν as 0.4, and noting that $b^2 \ll a^2$, these equations simplify to:

$$\sigma_r = \frac{0.668P}{t^2}\log_e\left(1.15\,\frac{a}{b}\right) \text{ at } r = 0 \qquad (6)$$

and

$$\sigma_r = \frac{0.668P}{t^2}\left[\log_e\left(0.490\,\frac{a}{r}\right) + 0.129\,\frac{b^2}{r^2}\right] \text{ at } r > b \qquad (7)$$

The deflection Δ of the centre of the disc is given by:

$$\Delta = \frac{3P\,(1-\nu^2)\,a^2}{4\pi E\,t^3} \qquad (8)$$

where E is Young's modulus.

The movement of the striker will be somewhat greater than Δ, since it will include a term for Hertzian indentation of the surface.

Consider the response of PA66 in the Montepolimeri test. The striker head has a radius of 10 mm, and the modulus of the polymer can be taken as 4 GPa at 23°C under impact conditions. The discs are 3.8 mm thick and clamped between rings of 30 mm radius. Under a load P of 800 N, the radius of Hertzian contact is 1.08 mm; the maximum stress σ_r, at r = 0, is 128 MPa; and the elastic deflection Δ is 0.66 mm. Montepolimeri obtained a figure of 125 MPa for the yield stress of dry nylon in tensile impact, whilst BASF measured a yield stress of 87 MPa after conditioning at 70°C and 65% RH, and it is therefore clear that a load of 800 N is sufficient to cause first yielding in the RP discs. Since the lowest peak load recorded by Montepolimeri in tests at 23°C is 1955 N, it is also clear that most of the PA66 discs reach first yield in the impact test and that the energy absorbed before first yield is a relatively small part of the total impact energy, even in relatively brittle failures. A similar conclusion was reached by Casiraghi, Castiglioni and Ajroldi in their study of the falling-weight impact behaviour of ABS over a range of temperatures (10).

In three-point bending, first yield causes an appreciable increase in specimen compliance and hence a deviation from linearity in the force-deflection curve. No comparable increase in compliance takes place in a centrally-loaded disc and the force-deflection relationship continues to follow equation (7), to a good approximation, until either the specimen fractures or general yielding begins.

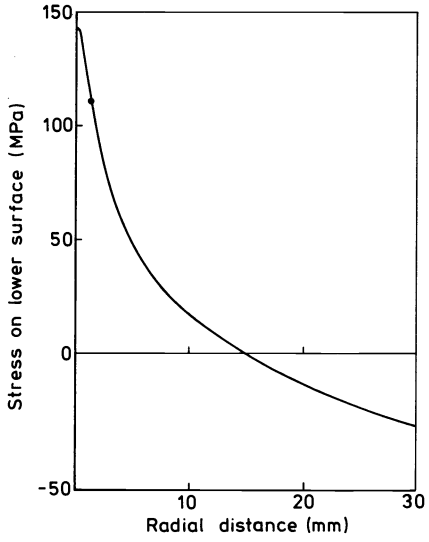

Fig. 22 Distribution of radial stress as a function of distance from the centre of a 3.8 mm thick PA66 disc clamped at 30 mm radius. Calculated from Eqn. (6), using E = 4 GPa, for the case of Δ= 1 mm at centre of disc. ● = radius of Hertzian contact.

The distribution of stresses across the disc represented by equation (6) is shown in Fig. 22. Near the centre of the disc, the lower surface is in tension but over the outer part of the disc the upper surface is in tension. Continued deflection by the striker increases both the total stored elastic energy and the level of stresses across the disc. If defects, such as weld lines or ejector pin marks, coincide with the region of high stress, the specimen will tend to respond by catastrophic crack propagation. The concentric cracks reported above in PA66 are an example of fracture initiated on the upper face of the disc from ejector pin marks on the outer part of the specimen.

Yielding

The sequence of events following first yield is complex, and no attempt will be made here to develop a quantitative treatment. However, it may be noted that the load acting on a ductile specimen can continue to increase as the area in contact with the striker increases, until eventually a hemispherical yielded region is formed. This condition will normally define the maximum attainable peak load, although, in principle, the resistance of the material can increase further as a result of strain hardening.

Fracture initiated either within the plastically deformed material or in the elastic region will terminate the absorption of impact energy and it is obvious from the data given in this paper that both weld defects and ejector pin marks cause premature tearing or cracking. Since all of the specimens tested fractured after first yield, the problem is not amenable to a conventional fracture mechanics analysis. However, fracture mechanics, together with microscopy, can quantify the effect of a weld or other flaw by equating it with an equivalent crack and thus provide a means for assessing the probable reduction in impact resistance in service.

DISCUSSION

The fracture mechanics results obtained in this programme illustrate, once again, the difficulties in making reproducible measurements of G_{IC} and K_{IC} in impact. A similar problem was encountered in an earlier study of polypropylene homopolymer and copolymer. Some of these problems can perhaps be attributed to differences in specimen preparation and testing procedure between different laboratories, but the major source of variation appears to be the scatter inherent in the energies to fracture of notched three-point bend specimens under impact loading.

A second problem affecting the fracture mechanics data is the establishment of valid conditions for plane strain fracture, especially as specimen sizes are limited in the case of bars machined from injection moulded plaques. The problems are less severe in impact then at low rates of strain but it is necessary to check the validity of the data in each case.

The use of impact energy tests on unnotched specimens, together with independently measured values of G_{IC}, to assign an equivalent crack size to a weld line or other surface defect is open to criticism, especially in the more ductile polymers. At small crack lengths, below about 1 mm, plasticity effects can become significant. Yielding at the crack tip not only increases the effective crack length, but can also lead to slow crack growth under conditions of increasing crack propagation resistance R, before catastrophic fracture begins. Nevertheless, despite these problems, there are advantages in being able to define the severity of a defect in quantitative terms.

The analysis of the response of discs to impact has concentrated on the purely elastic region and has shown that first yield occurs on the opposite face to the striker in even the most brittle specimens tested. Some very localised plastic yielding is also to be expected where the disc is in contact with the striker. It is possible that a certain amount of slow crack growth occurs from the weld before first yield is reached but the stored energy available is not sufficient to cause catastrophic fracture in this geometry. Only at much higher energies is such fracture observed. Montepolimeri comment that the number of fragments formed in brittle fracture of PA66 discs increases with the energy at break.

The analysis of deformation and failure in discs that have undergone substantial yielding presents severe difficulties that have not yet been satisfactorily addressed. The most successful study in this area is by Nimmer (11), who used an elastic-plastic finite element model, incorporating a strain hardening term, to predict the response of a polycarbonate disc. This model gave a good approximation to the force-deflection curve, but underestimated the load at rupture by about 40%.

It is interesting to note that PA66 actually has a higher K_{IC} than HDPE, but shows a high proportion of brittle fractures, whereas HDPE is essentially ductile. The difference is clearly due to the lower yield stress of HDPE, which is able to yield and draw before crack growth can become critical.

CONCLUSIONS

The following conclusions can be drawn from this study:

1. The measurement of G_{IC} and K_{IC} for HDPE and PA66 in impact presents problems of reproducibility between laboratories that require further elucidation but might prove to be inherent in the test.

2. Charpy measurements on unnotched bars can be used to define an effective crack length that is equivalent to a weld or other defect. Estimated values of effective crack length in PA66 specimens containing welds are in satisfactory agreement with the dimensions of weld line structures observed in the optical microscope.

3. Peak loads in dart impact tests on HDPE, PP, and PA66 are in all cases higher than those to produce first yield in the specimen.

4. In Type I RP plaques (head-on flow), weld lines reduce the impact energy of HDPE and PA66. A similar weakening is observed in ICI double edge gated plaques of polypropylene homopolymer and copolymer. Type II RP plaques show no such weakness.

5. In HDPE, yield occurs well before any crack can reach a critical size, whereas in PA66 the conditions necessary to produce general yielding are close to those required for catastrophic crack propagation from surface defects.

REFERENCES

1. S. Turner, Pure Appl. Chem. 52, 2739 (1980).
2. C. B. Bucknall, Pure Appl. Chem. to be published.
3. T. Casiraghi and S. Savadori, Plast.Rubb.Mater.Appl. 5 1 (1980).
4. T. Casiraghi, Poly.Eng.Sci., in press, 23, 902 (1983).
5. E. Plati and J.G. Williams, Poly.Eng.Sci., 15, 470 (1975).
6. M. K. V. Chan and J. G. Williams, Poly.Eng.Sci., 21, 1019 (1981).
7. C. B. Bucknall and P. Galloway, unpublished work.
8. S. P. Timoshenko and J. N. Goodier, Theory of Elasticity, 3rd edn. McGraw-Hill, New York (1970).
9. R. J. Roark and W. C. Young, Formulas for Stress and Strain 5th edn., McGraw-Hill, New York, 1975.
10. T. Casiraghi, G. Castiglioni and G. Ajroldi, Plast.Rubb.Proc. Appl. 2, 353 (1982).
11. R. P. Nimmer, Poly.Eng.Sci., 23, 155 (1983)